Powder Technology 318 (2017) 282–292

Contents lists available at ScienceDirect

Powder Technology

journal homepage: www.elsevier.com/locate/powtec

Coarse-grained discrete particle simulations of particle segregation in rotating fluidized beds in vortex chambers

Vikrant Verma [a,*], Tingwen Li [a,b], Juray De Wilde [a,c]

[a] National Energy Technology Laboratory, US Department of Energy, 3610 Collins Ferry Rd, Morgantown, WV 26507-0880, USA
[b] AECOM, Morgantown, WV 26505, USA
[c] Université catholique de Louvain, Materials and Process Engineering (IMAP), Place Sainte Barbe 2, 1348 Louvain-la-Neuve, Belgium

ARTICLE INFO

Article history:
Received 13 December 2016
Received in revised form 30 March 2017
Accepted 17 May 2017
Available online 26 May 2017

Keywords:
Rotating fluidized bed
Vortex chamber
Segregation
Discrete particle method
Coarse-grained DPM

ABSTRACT

Vortex chambers allow the generation of rotating fluidized beds, offering high-G intensified gas-solid contact, gas-solids separation and solids-solids segregation. Focusing on binary particle mixtures and fixing the density and diameter of the heavy/large particles, transient batch CFD-coarse-grained DPM simulations were carried out with varying densities or sizes of the light/small particles to evaluate to what extent combining these three functionalities is possible within a vortex chamber of given design. Both the rate and quality of segregation were analyzed. Within a relatively wide density and size range, fast and efficient segregation takes place, with an inner and slower rotating bed of the lighter/small particles forming within the outer and faster rotating bed of the heavier/large particles. Simulations show that the contamination of the outer bed with lighter particles occurs more easily than contamination of the inner bed with heavier particles and increases with decreasing difference in size or density of the particles. Bubbling in the inner bed is observed with an inner bed of very low density or small particles. Porosity plots show that vortex chambers with a sufficient number of gas inlet slots have to be used to guarantee a uniform gas distribution and particle bed. Finally, the flexibility of particle segregation in vortex chambers with respect to the gas flow rate is demonstrated.

1. Introduction

Already studied in the late sixties for biomass drying [1,2] and nuclear reactor applications [3–6], vortex chamber generated rotating fluidized beds have gained attention recently because of the process intensification potential resulting from high-G operation [7–12]. The high G-operation was shown to allow dense and more uniform beds at high slip velocities and the use of a wide range of particles, including large Geldart D-type and fine Geldart C-type particles. The bed rotation being driven by the tangential gas injection leads to a high flexibility with respect to the gas flow rate, but requires a careful vortex chamber design. The gas injection velocity has to be sufficiently high to generate enough centrifugal force to counteract the radial gas-solid drag force and prevent solids losses via the central gas outlet or chimney. This can be achieved by reducing the number of gas inlet slots or their size. Gas inlet slots smaller than the particles cause, however, inefficient transfer of tangential momentum to the bed and generate rotational motion of the particles around their own center of gravity. Reducing the number of slots is somewhat detrimental for the bed uniformity, but is frequently done for practical reasons. Another important design parameter is the chimney diameter which must be optimum and sufficiently far in order to allow the Coriolis force return the particles to the bed before being lost into the chimney. More details can be found in De Wilde et al. [12].

Several applications of rotating fluidized beds in vortex chambers have been studied. The intensification of interfacial mass, heat and momentum transfer opens perspectives for developing more compact particle dryers and the drying of biomass has been studied by several groups [1–2,7–8,13–14]. Particle coating and agglomeration has been studied more recently and involves the introduction of a dispersed liquid phase [15]. Multi-zone operation has been considered for both drying and coating/granulation applications as it allows short contact of the particles with a (very) hot gas. The dense and more uniform beds and high slip velocities are also promising for intensifying heterogeneous catalytic or non-catalytic reactions [10–11,16–18]. Two aspects are of particular importance. One is that, because of the relatively thin beds and high gas velocities, the gas phase residence time in the bed or gas-solid contact time is (extremely) short, while the solids residence time can normally be independently controlled by means of separated solids outlets. A second is that high gas flow rates can be applied without losing the bed, allowing to supply or evacuate significantly more heat via the gas than in conventional fluidized beds, e.g. of importance for carrying out strongly exothermic reactions [19–20].

* Corresponding author.
E-mail address: dr.v.vikrant@gmail.com (V. Verma).

http://dx.doi.org/10.1016/j.powtec.2017.05.037
0032-5910/

Using vortex chamber generated rotating fluidized beds to combine high-G intensified gas-solids contact and gas-solids separation with high-G intensified segregation was only recently considered and can be of importance for the development of an efficient reactor for oxy-fuel or chemical looping combustion of coal/biomass with in-situ ash separation that could be more easily operated at high pressure. In an experimental study of low-temperature wet coating of cohesive particles in a vortex chamber, segregation of non-coated and coated particles was observed. De Wilde et al. [21] presented CFD-DPM simulations to demonstrate the potential. A follow-up experimental study focusing on segregation was presented by Weber et al. [22] and confirmed combining high-G intensified gas-solids contact, gas-solids separation and solids-solids segregation is possible. In the present work, detailed CFD-coarse-grained DPM simulations are carried out to gain insight in the segregation behavior and in the flexibility with respect to the particle properties. The flexibility with respect to the gas flow rate is also addressed.

2. Discrete particle model

The MFIX-DPM code, developed at US Department of Energy's National Energy Technology Laboratory (NETL) is used to conduct the numerical simulations. In MFIX-DPM, DPM for the solid particles is coupled with the CFD flow solver to simulate the gas-solid flow. The gas phase is considered as the continuous phase whereas the particle trajectories are obtained by integrating Newton's equations of motion. The total force acting on individual particles is evaluated and the resulting accelerations, velocities and positions are tracked in time. The particle-particle collisions are directly resolved using a soft-sphere model [23–24] (based on a linear spring-dashpot model), which treats the collision as a continuous process taking place over a finite time. A four-way coupling is embedded to account for the effects of both phases on one another because of the relatively high solid concentrations in the dense gas-solid beds. Details on the model and governing equation can be found in Garg et al. [25]. The MFIX-DPM code was previously described and validated [28–29]. Among the advantages of the DPM model is the relative ease of incorporating an arbitrary distribution of particle properties, like size and density. Therefore DPM is preferred to study poly-dispersed particle flows. Tracking individual particles is, however, computationally expensive. To reduce the computational cost, the coarse-grained particle method was developed in which DPM particles are simulated as parcels [26]. Details of the method and its validations are described in Lu et al. [27]. Prior to applying the coarse-grained DPM method for the simulation of a bi-disperse rotating fluidized bed in a vortex chamber, additional verification and testing were carried out by comparing simulations with the original DPM and the coarse-grained particle models for both mono-disperse and bi-disperse systems. An example of the comparison of the calculated behavior with DPM and coarse-grained DPM for a binary mixture of 200 and 400 μm particles is given as on-line supplemental material to the paper. The agreement between DPM and coarse-grained DPM was found acceptable, especially in view of the sharply reduced calculation time. When e.g. parcels with a diameter double that of the actual particles are used in the coarse-grained DPM, the particle count is reduced to 0.72 million from 5.7 million with DPM. This results in a sharp reduction of the computation time to 20.6 h on 72 processors, compared to 200 h on 128 processors with DPM.

Several research groups used the DPM model to study segregation in conventional fluidized beds with mixtures of particles of different size and/or density [30–33]. Bokkers et al. [31] successfully predicted experimentally measured segregation rates in bi-disperse beds. A DPM-CFD model with periodic boundary conditions for the front and rear walls was developed by Feng et al. [32] to study the segregation and mixing of binary mixtures in a gas-fluidized bed of large thickness. DPM simulations of monodisperse, binary and ternary systems were presented by Tagami et al. [34]. The use of DPM to investigate the influence of fines on the segregation behavior of binary mixtures was addressed by Norouzi et al. [36]. A novel Lagrangian particle tracking method was used by Farzaneh et al. [35] to study mixing of fuel particles in fluidized beds. Recently, De Wilde et al. [21] used MFiX-DPM for the simulation of mono- and bi-disperse rotating fluidized beds in a vortex chamber and to demonstrate high-G intensification of particle segregation.

3. Simulations conditions

In this study we have considered the same geometry as in De Wilde et al. [21], shown in Fig. 1. The vortex chamber is 5 cm long (L_{vc}) and 24 cm in diameter (D_{vc}). The gas enters through 8 tangential gas inlet slots, 4 mm wide each, and is evacuated via an 8 cm diameter centrally positioned chimney. Details and dimensions of the geometry are given in Table 1. CAD software is used to draw the actual vortex chamber geometry. It generates the STL file containing the information on the walls of the vortex chamber. The vortex chamber geometry is then described in MFiX by the Cartesian cut-cell technique [37], tracing the STL geometry over a rectangular Cartesian background mesh. For details on the methodology, the simulated geometry and the choice of the operating conditions, readers are referred to De Wilde et al. [21]. The dotted line in Fig. 1 represents the rectangular block used in MFiX. In the present work, the transient segregation behavior of a batch of particles is studied with the particle inlet and outlet closed. Simulations start from a well-mixed rotating fluidized bed with the particles rotating with the velocity of a mono-disperse bed of the heavy particles at the given conditions (Fig. 1). To generate the initial flow field for the segregation simulations, referred to as 'well-mixed', a preparatory simulation is carried out with the given conditions and imposing for the type 2 color-particles identical properties as for the type 1 (monodisperse). The latter results in a well-mixed bed of particles of type 1 and type 2 color. At time t° of the actual segregation simulation, the real properties of the particles of type 2 are imposed and the evolution of the bi-disperse system studied.

Binary particle systems with different particle sizes and density ratios were considered. The particle density ratio was varied between 1.125 and 10 and the particle diameter ratio was between 1.066 and 5. The overall solids volume in the chamber was maintained constant in all simulations. As operation is high-G, the effect of gravity is typically negligible [12]. Except in simulations to study the influence of the gas flow rate or the number of slots, gas is fed at 10 g/s through each inlet slot. As discussed in De Wilde et al. [21], this is close to the minimum gas flow rate requirement to keep the bed of given mass rotating at sufficient speed. Operation is then typically at 4 to 5G. Atmospheric pressure is imposed at the chimney outlet. The restitution coefficient, the friction coefficient, and the spring constant were assumed to be respectively 0.9, 0.1 and 100 kg/s^2, values used in previous studies [21]. Details of the DPM parameters and the particle properties are given in Table 1.

It is essential to evaluate quantitatively the solids separation/segregation of binary particle mixtures in the vortex chamber. Goldschmidt et al. [38] defined the degree of segregation in a bi-disperse fluidized bed in terms of the average axial position of the particles of given type in the bed. A similar definition is adopted, but the average radial position of the particles of given type (heavy/light, large/small) is considered and referred to as average particle height. In addition, the segregation is quantified and the rotating fluidized beds are characterized by means of the rate of segregation, the (tangentially averaged) fraction of light or small particles at a given radial position in the chamber, the particle bed rotation speed, and the particle number density and uniformity. The data presented are averaged in the axial direction. With the particle properties used, no significant differences in the bed rotation speed, density and composition were observed in this direction.

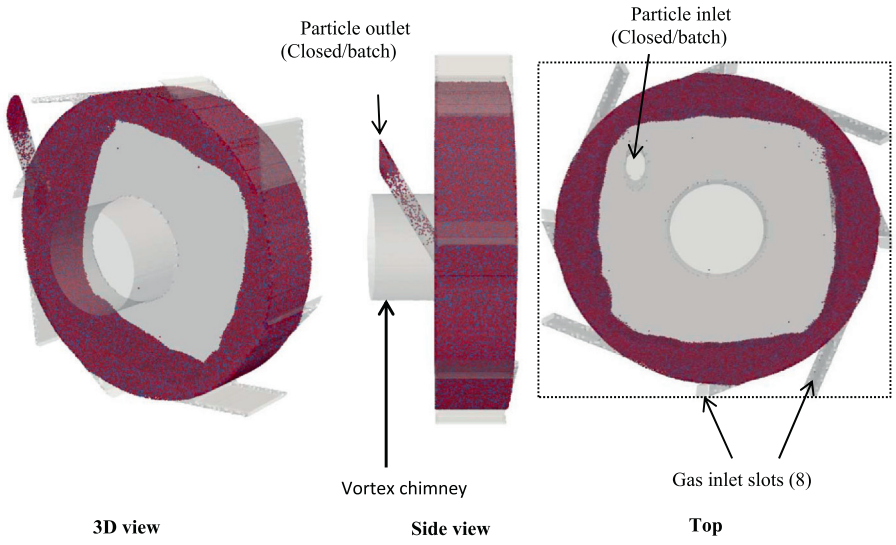

Fig. 1. Vortex chamber geometry with initial well-mixed bi-disperse rotating fluidized bed with the particles rotating with the velocity of a mono-disperse bed of the heavy particles. Particles of different density or diameter are colored red and blue. The dotted line in the top view represents the rectangular block used by MFiX in which the actual geometry is generated using a STL file. (For interpretation of the references to color in this figure legend, the reader is referred to the web version of this article.)

4. Results and discussion

Sections 4.1 and 4.2 discuss the effect of respectively the particle density and particle diameter ratio on the segregation in the vortex chamber. The influences of gas flow rate and of the number of gas inlet slots are reported in Sections 4.3 and 4.4. For visualization purposes and throughout this study, the heavy/large and lighter/small particles are colored red and blue, respectively. Starting from a well-mixed rotating fluidized bed, simulations were continued until the steady state was reached, that is, no further change in the particle segregation and particle velocity profiles is observed.

Table 1
Vortex chamber dimensions and operating conditions used in the simulations.

	Symbol	Unit	Value
Geometry			
Vortex chamber diameter	D_{vc}	m	0.24
Vortex chamber length	L_{vc}	m	0.05
Chimney diameter	D_c	m	0.08
Number of gas inlet slots	n	–	8
Gas slot width (individual)	s	m	4×10^{-3}
System geometry	$L_x \times L_y \times L_z$	m × m × m	0.26 × 0.102 × 0.26
Eulerian grid	$dx \times dy \times dz$	–	178 × 81 × 178
Operating conditions/properties			
Gas density	ρ_g	kg/m^3 g	Uses ideal gas law (~1.2)
Gas phase viscosity	μ_g	Pa × s	1.8×10^{-5}
Particle density, type 1	ρ_{p1}	kg/m^3	2700
Particle diameter, type 1	d_{p1}	m	8×10^{-4}
Restitution coefficient	e	–	0.9
Friction coefficient	μ	–	0.1
Spring constant	k	kg/s^2	100
Gas flow rate	F_g	g/s	8 × 10 (base case)
Gas flow rate (ref. Section 4.3)	F_g	g/s	8 × 10, 8 × 20
Gas flow rate (ref. Section 4.4)	F_g	g/s	8 × 10, 7 × 10, 4 × 20
Particle density ratios (fixed diameter)	ρ_{p1}/ρ_{p2} ($d_{p1}/d_{p2} = 1$)	–	1.125, 1.22, 1.35, 2, 5, 10
Particle diameter ratios (fixed density)	d_{p1}/d_{p2} ($\rho_{p1}/\rho_{p2} = 1$)	–	1.06, 1.142, 1.33, 2, 3, 4, 5

4.1. Effect of the particle density ratio on segregation

Fixing the density of the heavy particles (type 1) at 2700 kg/m^3, the density of the light particles (type 2) was varied, with the particle density ratio reaching values up to 10. Segregation of particles is expected due to a difference in the centrifugal force acting on the particles of different densities. To get insight in the minimum density ratio required for efficient segregation, simulations with a small particle density ratio were also carried out, i.e. with $\rho_{p1}/\rho_{p2} = 1.125$, 1.227 and 1.35. Fig. 2 shows snapshots of the bi-disperse rotating fluidized bed after reaching steady state. Heavy and light particles are colored red and blue respectively. The square shaped particle bed is discussed later in this section, segregation is focused on first. The latter is seen to improve with increasing particle density ratio. With a particle density ratio of 1.125, segregation of particle is seen to be ineffective. Only a thin inner layer of light particles is formed and the heavy particle bed is largely contaminated with light particles. As the particle density ratio increases from 1.125 to 1.35, segregation takes place and a thicker inner layer of light particles is formed. Contamination of the outer bed of heavy particles with light particles remains, however, significant. A quantitative picture of the fraction light particles in the bed as a function of the radial position is shown in Fig. 3 and confirms contamination of the outer and inner bed with light/heavy particles at the lower particle density ratios of 1.125 to 1.35. With particle density ratios above 2, a pure inner bed of light particles and an outer bed consisting of >95% of heavy particles are formed. The total bed thickness of only 3 to 5 cm should be kept in mind. The interface between the outer and inner beds of heavy and light particles is positioned at r/R = 0.82 approximately. Fig. 3 cannot be extended to lower r/R because insufficient particles are present in the inner region to calculate meaningful values of segregation or of averages. Whereas the thickness of the outer bed is hardly affected by the particle density ratio, the thickness of the inner bed is seen to increase with increasing particle density ratio. The increase in inner bed thickness (or height in the radial direction) reflects the radial fluidization of the inner bed of lighter particles. Within the range studied, no significant losses of light particles via the chimney were, however, observed. Only at the higher particle density ratios (>2), some light particles were lost through the chimney. In their experiments on coating of cohesive particles in a vortex chamber Eliaers et al. [13] observed significant losses of uncoated particles, the much heavier coated particles staying

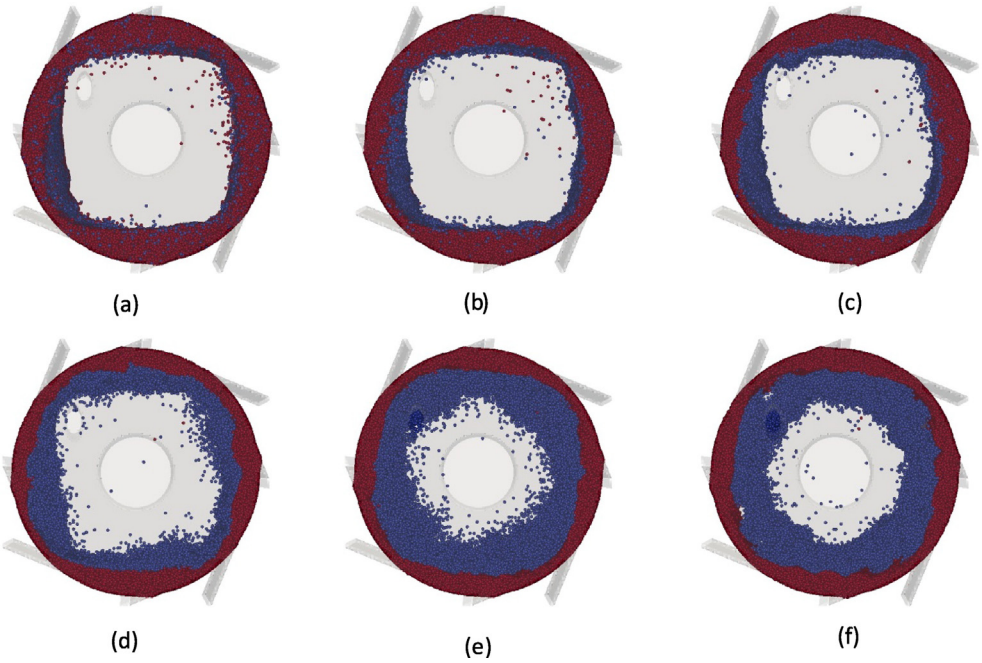

Fig. 2. Snapshots of the bi-disperse rotating fluidized bed after reaching steady state, showing the effect of the particle density ratio (ρ_{p1}/ρ_{p2}) on segregation. Simulations with ρ_{p1}/ρ_{p2} of (a) 1.125, (b) 1.227, (c) 1.35, (d) 2.0, and (e) 5.0 and (f) 10.0. The heavy particles (ρ_{p1} = constant) are colored red, the light particles (ρ_{p2} = varied) blue. (For interpretation of the references to color in this figure legend, the reader is referred to the web version of this article.)

inside the chamber. Fig. 2 shows that with the highest particle density ratios of 5 and 10, that is, with the lightest light particles, the formation of bubbles is observed. The formation of bubbles causes some mixing of light particles into the outer bed of heavy particles, as can be clearly seen in Fig. 3. At the highest particle density ratio of 10, some mixing of heavy particles into the inner bed of light particles is also observed. The simulations are in line with observations by several groups with mono-disperse rotating fluidized beds in vortex chambers, showing that a dense and uniform particle bed is not always obtained and bubbling and solids losses via the chimney can occur, especially with light particles [12]. With mono-disperse particles, the vortex chamber design can, however, be optimized to minimize bubbling. Using smaller or less slots in order to increase the gas injection velocity for given gas flow rate and as such increasing the ratio of the generated centrifugal force-to-radial gas-solid drag force on a single particle was shown to be efficient within a given range [12]. Using slots much smaller than the particles has to be avoided, however, as this generates rotational

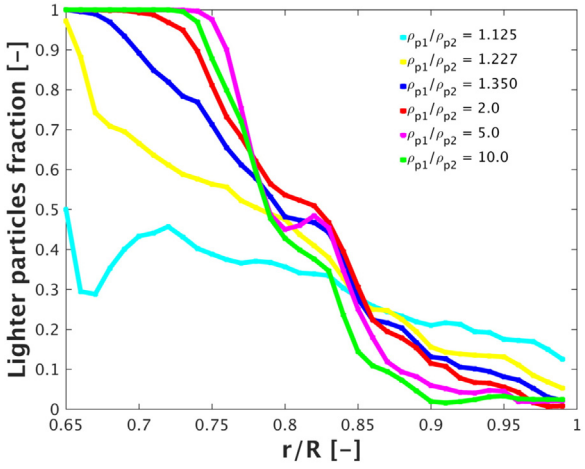

Fig. 3. Snapshot of the radial profiles of the light particle fraction in the bi-disperse rotating fluidized bed after reaching steady state. Comparison for different particle density ratios (ρ_{p1} = constant, ρ_{p2} = varied).

motion of the particles around their own center of gravity and related energy dissipation. With bi-disperse particle mixtures, the design of the vortex chamber typically accounts for the characteristics of the particles in the outer bed in the first place. Accounting for the characteristics of the particles in the inner bed in the design of the vortex chamber is possible to a certain extent, but becomes the more challenging with strongly bi-disperse particle mixtures, in particular in case of a difference in particle diameter. Using a smaller diameter chimney allows particles to be returned to the bed by the Coriolis effect more efficiently and strengthen the central vortex, both reducing solids losses via the chimney. The presented simulations demonstrate that using a properly designed vortex chamber, high-G intensified gas-solids contact can be combined with high-G intensified gas-solids separation and solids-solids segregation and this in a relatively wide particle density difference range. The simulations also show that the quality of segregation, i.e. the purity of the formed beds, is optimal at a given particle density ratio, with the vortex chamber simulated and the imposed gas flow rate 2 to 5.

The particle bed uniformity cannot be accurately evaluated by means of the particle position plots shown in Fig. 2 only. Snapshots of the particle bed porosity after reaching steady state are shown in Fig. 4 for the different particle density ratios considered. The inner bed of light particles is relatively dilute and uniform. Only at the highest particle density ratios, bubbling is reflected in the inner bed porosity profile (Fig. 4e and f). In the outer bed of heavy particles, a well-defined non-uniformity in the particle bed porosity/density is observed. Looking in the tangential/rotational direction, regions where the bed is nearly packed are altered with regions that are significantly less dense. CFD simulations of vortex chamber generated rotating fluidized beds using a Eulerian-Eulerian approach already revealed similar phenomena, especially with a small number of gas inlet slots (e.g. [39]). Particles being slowed down right upstream of a gas inlet slot (in the rotational direction) leads to densification and particles being accelerated right downstream of a gas inlet slot to bed dilution. The behavior is, however, more complex and a remarkable square shaped porosity profile is formed, as already observed in Fig. 2, despite the presence of 8 gas inlet slots. The profile probably reflects an eigenmode of the system. On first sight, two gas inlet slots are acting as one – which is not entirely

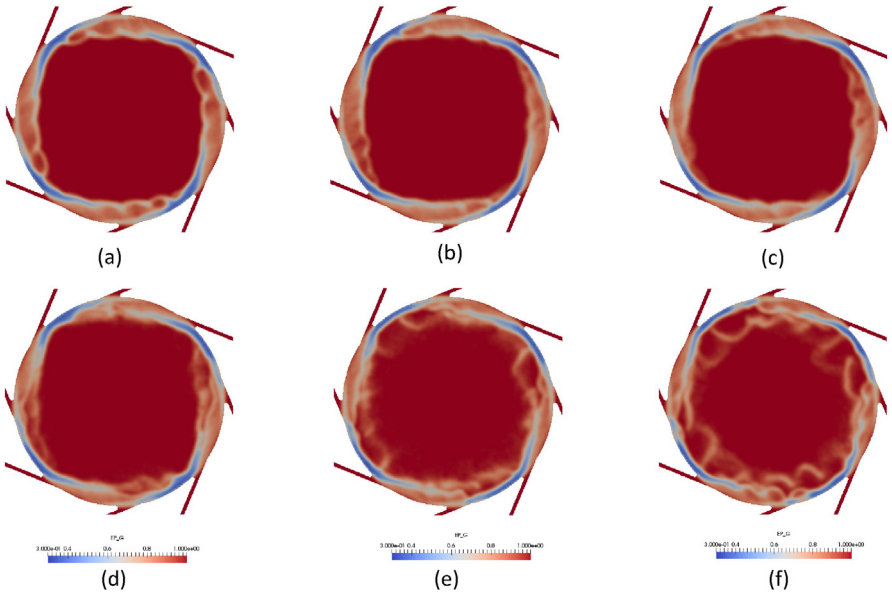

Fig. 4. Snapshots of the porosity after reaching steady state, showing the effect of the particle density ratio (ρ_{p1}/ρ_{p2}). Simulations with ρ_{p1}/ρ_{p2} of (a) 1.125, (b) 1.227, (c) 1.35, (d) 2.0, and (e) 5.0 and (f) 10.0 (ρ_{p1} = constant, ρ_{p2} = varied). Blue and red colors represent the lowest and highest gas volume fraction of 0.3 and 1.0 respectively. (For interpretation of the references to color in this figure legend, the reader is referred to the web version of this article.)

the case as will be shown later. The impact of the gas flow rate and of the number of gas inlet slots on the presence of this eigenmode is discussed in more detail in Sections 4.3 and 4.4.

Figs. 5 and 6 focus on the transient behavior in the bi-disperse rotating fluidized bed, starting from a well-mixed bed as shown in Fig. 1. The evolution in time of the average radial position of particles of given type or 'average particle heights' and of the average velocity of particles of given type are shown for varying particle density ratio (ρ_{p1}/ρ_{p2}) in Figs. 5 and 6 respectively. The transient behavior provides additional information on the segregation rate or time scale and the effects of bubbling in the inner bed. The data confirm fast segregation, within 0.2 to 1 s depending on the particle density ratio. Segregation is not only more pronounced, but also faster with increasing particle density ratio (Fig. 5). The more pronounced decrease of the average particle height of the light particles than increase of the average particle height of the heavy particles with increasing particle density ratio is explained by the expansion of the inner bed. With particles of equal diameter but different densities, the radially inward gas-solid drag force on the particles of different types will be similar, whereas the radially outward centrifugal force will be significantly different. This explains the absence of bed expansion in the outer bed (constant ρ_{p1}) and the observed bed expansion in the inner bed, in particular at higher particle density ratio (variable ρ_{p2}). In the inner bed of light particles, fluctuations in the average particle height are also observed at higher particle density ratio, probably as a result of bubble formation.

During segregation, a difference in rotation speed between the outer bed of mainly heavy particles and the inner bed of mainly light particles builds up (Fig. 6), but the difference remains limited and less than about 20%. The average particle velocity in the outer bed is seen to become higher than the average particle velocity in the inner bed. This is on one hand due to the proximity of the outer bed to the gas inlet slots through which tangential momentum is provided and on the other

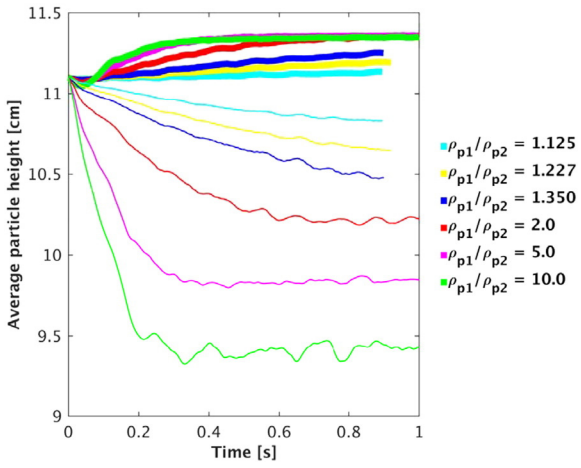

Fig. 5. Influence of the particle density ratio (ρ_{p1}/ρ_{p2}) on the evolution in time of the average radial position of particles of given type in the bi-disperse rotating fluidized bed, starting from a well-mixed rotating fluidized bed as shown in Fig. 1. Thick lines represent the heavy particles (ρ_{p1} = constant) whereas thin lines represent the light particles (ρ_{p2} = varied).

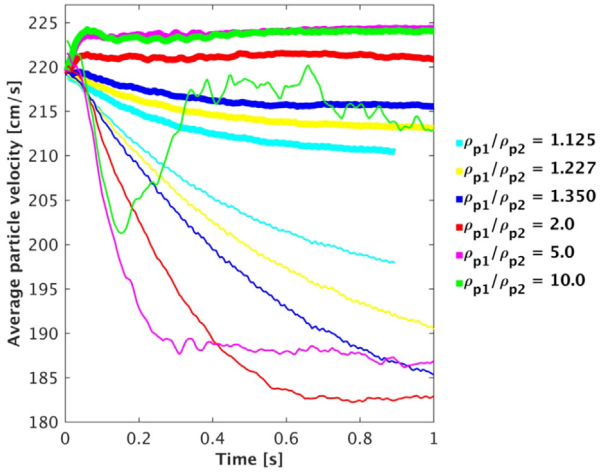

Fig. 6. Influence of the particle density ratio (ρ_{p1}/ρ_{p2}) on the evolution in time of the average velocity of particles of given type in the bi-disperse rotating fluidized bed, starting from a well-mixed rotating fluidized bed as shown in Fig. 1. Thick lines represent the heavy particles (ρ_{p1} = constant) whereas thin lines represent the light particles (ρ_{p2} = varied).

hand due to the typical solid body type behavior of rotating fluidized beds of sufficient density and uniformity [12]. Up to a particle density ratio of 2, the difference in rotation speeds between the outer and inner bed increases with increasing particle density ratio. At higher particle density ratio, when bubbling occurs (Fig. 2), the rotation speed of the inner bed of light particles is seen to increase. In their CFD-DPM simulations of a bi-disperse rotating fluidized bed in a vortex chamber, De Wilde et al. [21] observed a higher rotation speed of the inner bed of light particles. This is due to the much lower bed density in the inner bed than in the present simulations, allowing maintaining a stronger central vortex. With the initial particle velocities that of a monodisperse rotating fluidized bed of the heavy particles, the average particle velocities of both the heavy and light particles are seen to decrease in time at small particle density ratio ($\rho_{p1}/\rho_{p2} = 1.125$, 1.227 and 1.35). At higher particle density ratio ($\rho_{p1}/\rho_{p2} = 2$, 5 and 10), the average particle velocity of the heavy particles increases in time, whereas that of the light particles decreases until steady state values are reached.

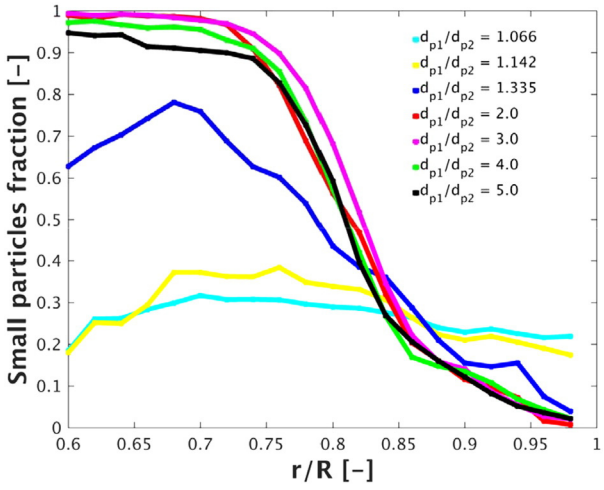

Fig. 8. Snapshot of the radial profiles of the light particle fraction in the bi-disperse rotating fluidized bed after reaching steady state. Comparison for different particle diameter ratios (d_{p1} = constant, d_{p2} = varied).

4.2. Effect of the particle size ratio on segregation

Particle size based segregation in a vortex chamber generated bi-disperse rotating fluidized bed was evaluated by keeping the particle diameter of the large particles (type 1) constant at 800 μm and varying the particle diameter of the small particles (type 2) so that the particle diameter ratio d_{p1}/d_{p2} was between 1.066 and 5.0. Three narrow particle diameter ratios between 1.066 and 1.335 were included. The overall behavior is similar as with particle density based segregation (Section 4.1), but some qualitative and quantitative differences are observed as discussed hereafter.

Snapshots of the bi-disperse rotating fluidized bed after reaching steady state are shown in Fig. 7 with the large and small particles colored red and blue respectively. The radial profiles of the fraction of small particles in the bed that are shown in Fig. 8 give a quantitative picture of the segregation. As expected, segregation becomes the more pronounced as the particle diameter ratio increases. With the particle diameter ratios d_{p1}/d_{p2} of 1.066 and 1.142, segregation is hardly observed. At $d_{p1}/d_{p2} = 1.335$, segregation starts, but the inner bed of small particles is significantly contaminated with large particles and vice versa. Efficient segregation is observed at $d_{p1}/d_{p2} = 2$–5, with the small particle fraction in the inner bed higher than 95% and that in part of the outer bed below 5%. A 100% purity of the inner or outer bed could, however, not be achieved within the 3 to 6 cm thick bed. Furthermore, an optimum particle diameter ratio exists. With the vortex chamber simulated and the imposed gas flow rate, the bed purity is highest with a particle diameter ratio of 2–3. At higher particle diameter ratio (4 and 5), the interface between the outer and inner bed becomes irregular, with somewhat wavy structures forming. This results in localized radial mixing of large and small particles (Fig. 7), detrimental for the quality of segregation (Fig. 8). The interface between the inner bed and the particle bed freeboard region is also seen to become more irregular. Together with the bed expansion with increasing particle diameter ratio, this leads to some solids losses via the chimney. At the highest particle diameter ratios, some bubble formation is observed, but much less pronounced than at high particle density ratio. This is also seen in the snapshots of the particle bed porosity after reaching steady state that are shown in Fig. 9 for the different particle diameter ratios studied.

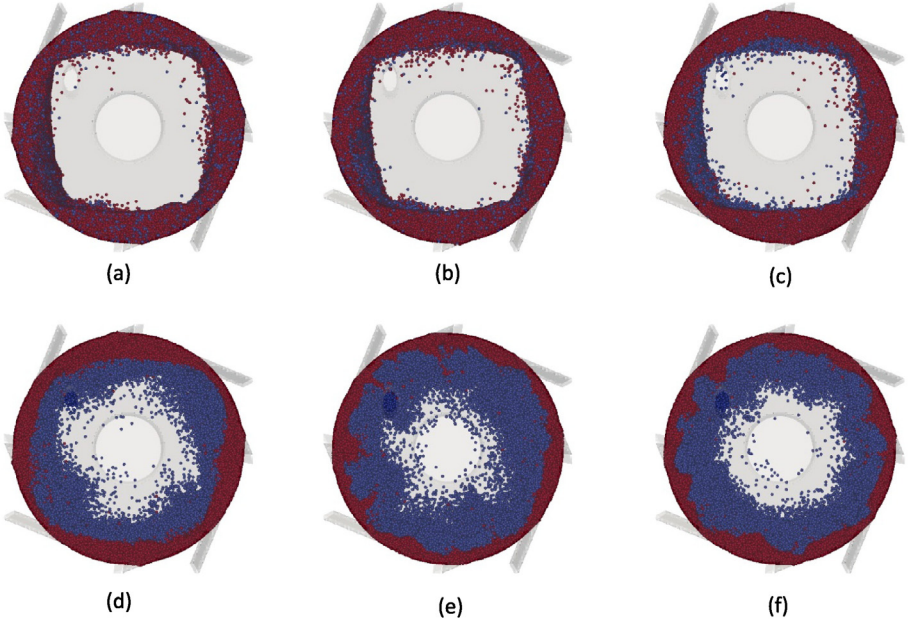

Fig. 7. Snapshots of the bi-disperse rotating fluidized bed after reaching steady state, showing the effect of the particle diameter ratio (d_{p1}/d_{p2}) on segregation. Simulations with d_{p1}/d_{p2} of (a) 1.066, (b) 1.142, (c) 1.335, (d) 2.0, and (e) 4.0 and (f) 5.0. The large particles (d_{p1} = constant) are colored red, the small particles (d_{p2} = varied) blue. (For interpretation of the references to color in this figure legend, the reader is referred to the web version of this article.)

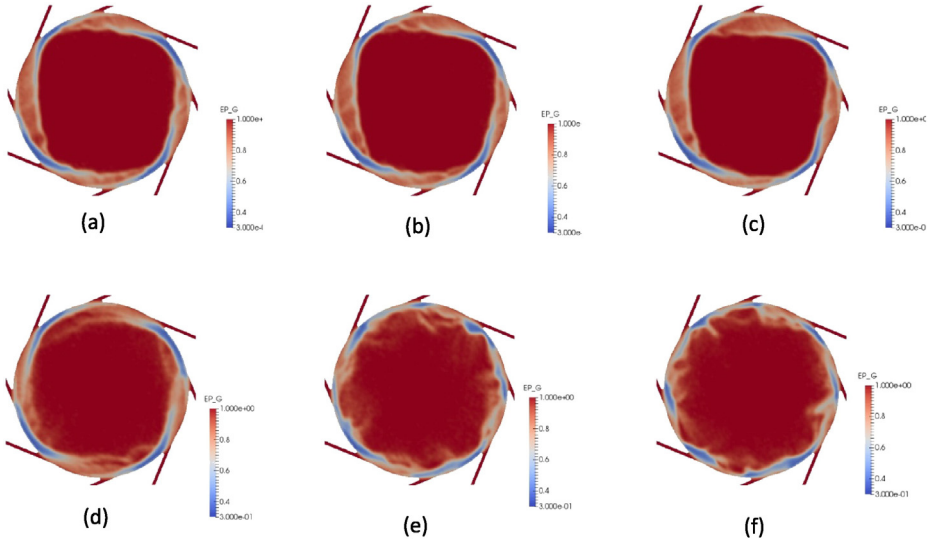

Fig. 9. Snapshots of the porosity after reaching steady state, showing the effect of the particle diameter ratio (d_{p1}/d_{p2}). Simulations with d_{p1}/d_{p2} of (a) 1.066, (b) 1.142, (c) 1.335, (d) 2.0, and (e) 4.0 and (f) 5.0 (d_{p1} = constant, d_{p2} = varied). Blue and red colors represent the lowest and highest gas volume fraction of 0.3 and 1.0 respectively. (For interpretation of the references to color in this figure legend, the reader is referred to the web version of this article.)

The inner bed of small particles is in all cases relatively dilute and uniform. The well-defined non-uniformity in the outer bed of large particles, i.e. the alternating regions of a nearly packed and significantly less dense bed leading to a square shaped particle bed (Fig. 7), is again observed for particle diameter ratios up to 2. At higher particle diameter ratio, as the interface between the outer and inner bed becomes irregular, the dominant square shape is lost. In the porosity profiles (Fig. 9f), this is reflected in the appearance of 8 instead of 4 particle bed density alternations in the periphery. When looking in the particle bed rotational direction, particles are decelerated right upstream and accelerated right downstream of a gas inlet.

The evolution in time of the average radial position of particles of given type or 'average particle heights' and of the average velocity of particles of given type, shown for varying particle diameter ratio (d_{p1}/d_{p2}) in Figs. 10 and 11 respectively, reveals significant qualitative and quantitative differences in the transient behavior of the bi-disperse rotating fluidized bed with particles of different diameters, compared to that with particles of different densities. Reaching the steady state is seen to take longer, minimum about 1 s, especially in the inner bed of small particles. Segregation is seen to be faster with increasing particle diameter ratio. Up to a certain particle diameter ratio, the average particle height of the outer bed is seen to increase with increasing particle diameter ratio and that of the inner bed decrease. As an outer and inner bed of large/small particles is formed, it is seen to accelerate and decelerate respectively from the velocity of the well-mixed bed that was initially imposed (Fig. 11). The steady state average particle velocity in the outer bed is seen to increase with increasing particle diameter ratio. The steady state average velocity in the inner bed reaches a minimum at given particle diameter ratio, under the conditions studied between 2 and 3. At higher particle diameter ratio, the steady state average particle velocity in the inner bed again increases, probably explained by the reduced density of the inner bed, allowing a stronger central vortex. The deceleration of the inner bed is accompanied by bed expansion, reflected in the decrease of the average particle bed height of the small particles (Fig. 10). At higher particle diameter ratio (d_{p1}/d_{p2} = 3–5), the average particle height and average particle velocity of the inner bed of small particles are seen to rapidly decrease, go through a minimum and then increase again to their steady state values where

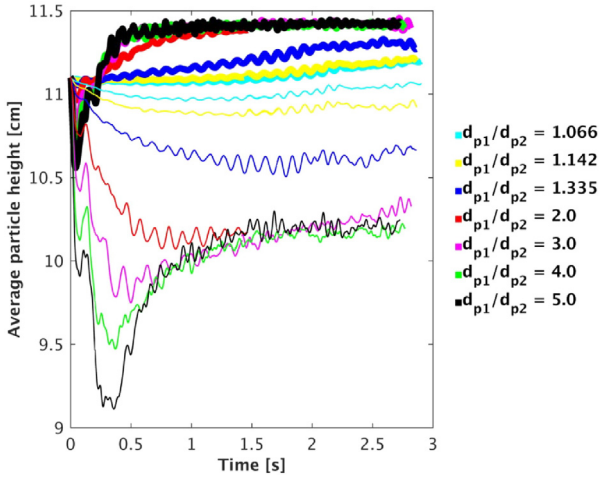

Fig. 10. Influence of the particle diameter ratio (d_{p1}/d_{p2}) on the evolution in time of the average radial position of particles of given type in the bi-disperse rotating fluidized bed, starting from a well-mixed rotating fluidized bed as shown in Fig. 1. Thick lines represent the large particles (d_{p1} = constant) whereas thin lines represent the small particles (d_{p2} = varied).

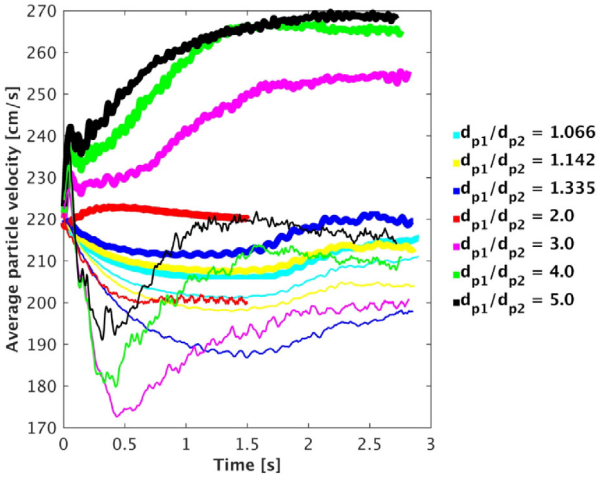

Fig. 11. Influence of the particle diameter ratio (d_{p1}/d_{p2}) on the evolution in time of the average velocity of particles of given type in the bi-disperse rotating fluidized bed, starting from a well-mixed rotating fluidized bed as shown in Fig. 1. Thick lines represent the large particles (d_{p1} = constant) whereas thin lines represent the small particles (d_{p2} = varied).

the counteracting radial gas-solid drag force and the centrifugal force on the particles are equilibrated. The initial fast bed expansion and resulting bed dilution indeed cause the bed to re-accelerate and re-contract to a certain extent. The minimum in the average particle height of the small particles is seen to become the more pronounced with increasing particle diameter ratio (Fig. 10), whereas the minimum in the average velocity of the small particles is seen to be the most pronounced at a given particle diameter ratio, under the conditions studied (Fig. 11). After reaching the steady state, small fluctuations in the average particle height of both the inner bed of small particles and outer bed of large particles are observed. The fluctuations in the inner and outer bed are correlated, that is, their frequency is identical, but the fluctuations in the inner bed are somewhat more pronounced, probably because of the contact of the outer bed with the cylindrical wall. The observed fluctuations can be at the origin of exchange of small and large particles between the outer and inner beds.

4.3. Effect of the gas flow rate

Vortex chamber generated rotating fluidized beds of mono-disperse particles are known to be flexible with respect to the gas flow rate, the latter affecting the centrifugal force and counteracting radial gas-solid drag force in similar ways [12]. As such, the concepts of minimum fluidization velocity and terminal velocity of the particles cannot be used and in a relatively wide gas flow rate range, the bed height is seen to be not much affected by the gas flow rate. The flexibility with respect to the gas flow rate opens perspectives for applications requiring a high gas throughput or extremely short gas phase residence time. With a bi-disperse rotating fluidized bed, the flexibility of the segregation with respect to the gas flow rate can be questioned. Figs. 12, 13 and 14 show the effect of doubling the gas flow rate for the given conditions, Fig. 12 for $\rho_{p1}/\rho_{p2} = 2$, Figs. 13 and 14 for $\rho_{p1}/\rho_{p2} = 2$ and $d_{p1}/d_{p2} = 2$. The snapshots of the steady state particle positions shown in Fig. 12a–b confirm the flexibility with respect to the gas flow rate. No expansion of the outer bed and a minor expansion of the inner bed are observed when doubling the gas flow rate. This confirms a similar influence of the gas flow rate on the centrifugal force and the counteracting radial gas-solid drag force, as previously reported for mono-disperse particles [12]. Furthermore, the quality of segregation is roughly maintained. Similar observations were made with $d_{p1}/d_{p2} = 2$, with the inner bed of small particles being somewhat better confined at higher gas flow rate. Note that when doubling the gas flow rate, the square shaped form of the particle bed is less dominant in the outer bed and has completely disappeared in the inner bed. This confirms that the

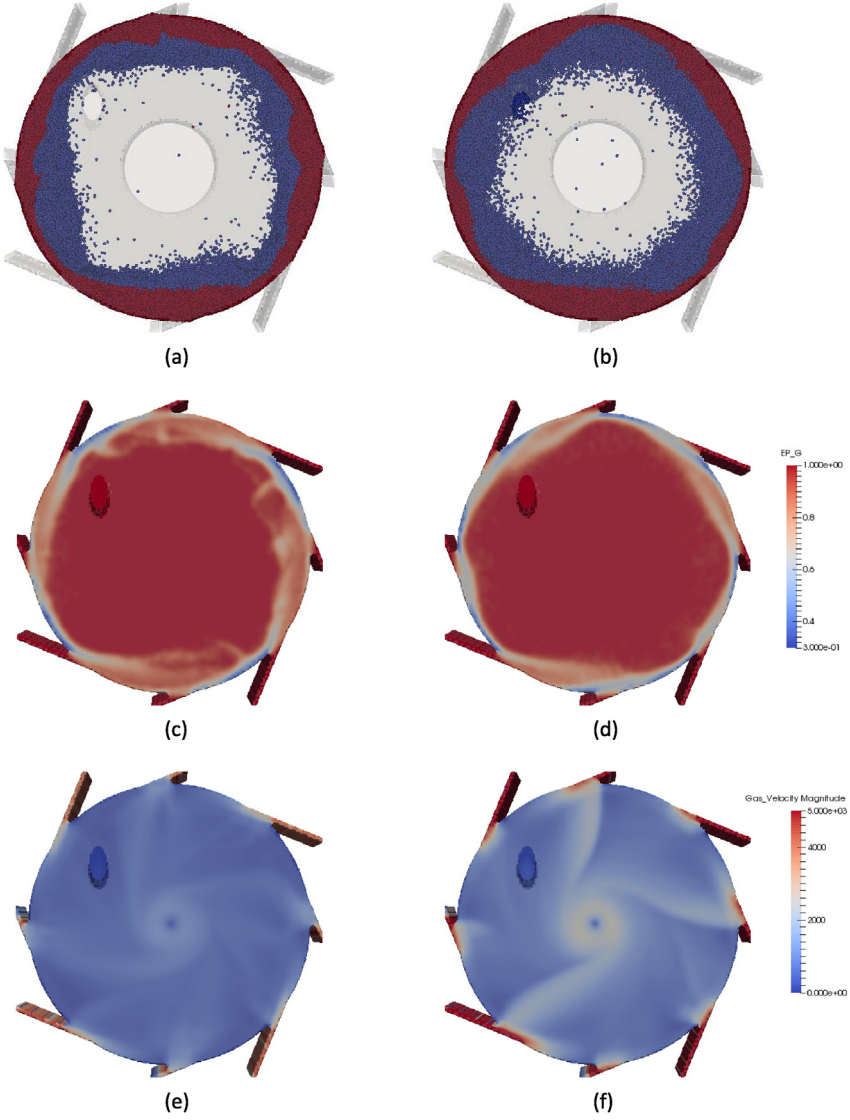

Fig. 12. Influence of the gas flow rate on the steady state profiles of the (a, b) particle positions and segregation, (c, d) bed porosity, and (e, f) gas velocity (snapshots shown). Case study with a gas flow rate F_g of (a, c, e) 8 × 10 g/s and (b, d, f) 8 × 20 g/s and with a particle density ratio (ρ_{p1}/ρ_{p2}) of 2.0.

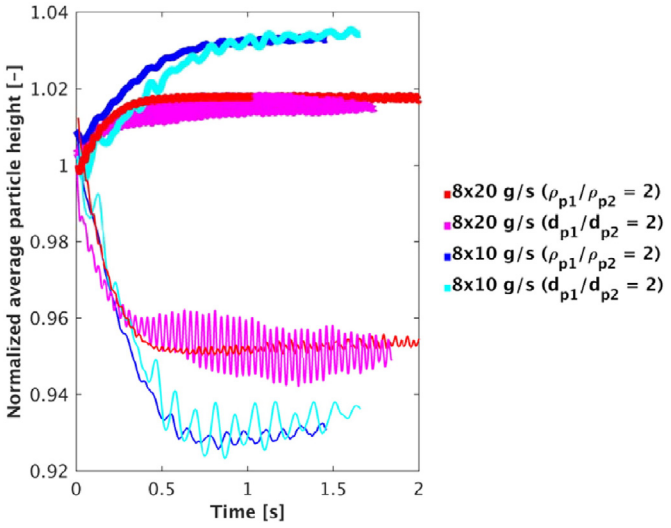

Fig. 13. Influence of the gas flow rate on the evolution in time of the normalized average radial position of particles of given type in the bi-disperse rotating fluidized bed, starting from a well-mixed rotating fluidized bed as shown in Fig. 1. Thick lines represent the heavy or large particles (type 1) whereas thin lines represent the light or small particles (type 2). Case studies with a gas flow rate F_g of 8 × 10 g/s and 8 × 20 g/s and with a particle density ratio (ρ_{p1}/ρ_{p2}) or a particle diameter ratio (d_{p1}/d_{p2}) of 2.0.

reference gas flow rate studied in this work is close to the minimum gas flow rate required for stable operation, as explained in De Wilde et al. [21]. The porosity plots shown in Fig. 12c–d confirm a minor influence of the gas flow rate on the particle bed density and a favorable effect on the bed uniformity. Fig. 12e–f shows that when moving radially inward, the gas velocity on the one hand decreases because of the reducing solids volume fraction, but on the other hand increases because of the decreasing circumference. The net effect is a relatively smooth evolution of the gas velocity. The evolution in time of the normalized average particle heights shows faster segregation at higher gas flow rate (Fig. 13). Both with a bi-disperse bed with $\rho_{p1}/\rho_{p2} = 2$ and $d_{p1}/d_{p2} = 2$, the average particle height of the heavy particles slightly decreases, whereas that of the light particles slightly increases when reaching the steady state, so that heavy and light particles come somewhat closer

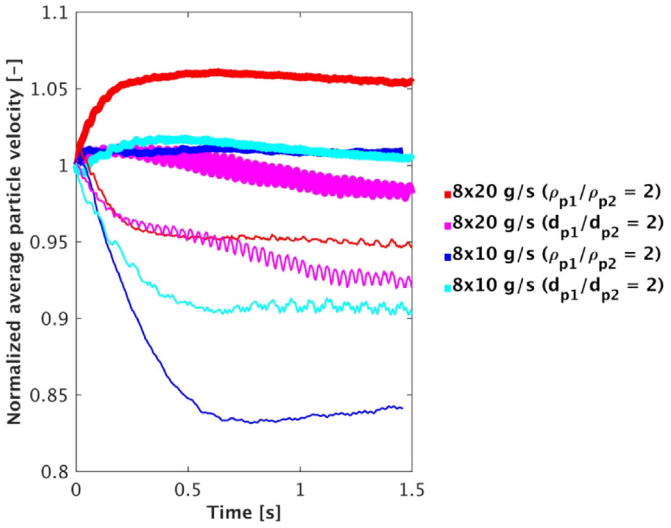

Fig. 14. Influence of the gas flow rate on the evolution in time of the normalized average velocity of particles of given type in the bi-disperse rotating fluidized bed, starting from a well-mixed rotating fluidized bed as shown in Fig. 1. Thick lines represent the heavy or large particles (type 1) whereas thin lines represent the light or small particles (type 2). Case studies with a gas flow rate F_g of 8 × 10 g/s and 8 × 20 g/s and with a particle density ratio (ρ_{p1}/ρ_{p2}) or a particle diameter ratio (d_{p1}/d_{p2}) of 2.0.

together. Quantitatively, the influence of the gas flow rate on the average particle bed heights is seen to be similar with $\rho_{p1}/\rho_{p2} = 2$ and with $d_{p1}/d_{p2} = 2$. Whereas the amplitude is hardly influenced, the frequency of fluctuations in the average particle heights is seen to be doubled when doubling the gas flow rate, indicating a relation between the fluctuations and the particle bed rotational motion. The influence of the gas flow rate on the evolution in time and steady state of the normalized average particle velocities (Fig. 14) shows a more complicated picture. With a bi-disperse bed with $\rho_{p1}/\rho_{p2} = 2$, the steady state normalized average particle velocity of both the heavy and light particles increases with increasing gas flow rate and the increase is somewhat more pronounced in the inner bed of light particles, indicating formation of a stronger central vortex. With $d_{p1}/d_{p2} = 2$, the steady state normalized average particle velocity of the large particles slightly decreases, whereas that of the small particles slightly increases. This difference in behavior is explained by the different effect of the gas flow rate on the drag and centrifugal forces for particles of different density or size. In any case, the difference in rotation speed between the outer and inner bed decreases with increasing gas flow rate. With $d_{p1}/d_{p2} = 2$, small fluctuations in the average particle velocity of the large particles in the outer bed, similar to those existing in the inner bed of small particles, appear at higher gas flow rate.

4.4. Effect of the number of gas inlets

Experimental studies with different types of particles showed the importance of the vortex chamber design, i.e. the number of slots and their size, for optimizing the solids retention and efficiently generating a rotating fluidized bed of particles of given type [17,18]. Reducing the number of gas inlet slots or their size allows increasing the gas injection velocity for given gas flow rate and as such the ratio of the generated single particle centrifugal force-to-radial gas-solid drag force, the latter being determined by the gas flow rate only. This ratio will determine the bed density that can be achieved with given solids loading and gas flow rate. A too strong reduction of the number of gas inlet slots or a too strong increase of the gas injection velocity can, however, be detrimental for the transfer of tangential momentum between the injected gas and the particle bed and for the particle bed density and uniformity. Gas inlet slots much smaller than the particles are also to be avoided, as the contact between the gas inlet jets and the particles then generates significant rotation of the particles around their own center of gravity [12,21]. When the bed is radially fluidized and the particles are retained in the chamber, as is the case in the simulations presented, the centrifugal force compensates for the radial gas-solid drag force, so that the ratio is 1. The issue is then at what bed rotation speed and related bed density this force balance is achieved. With increasing solids loading and given gas flow rate, for example, a force balance will typically be reached at lower bed density.

The simulations presented in this section study on the one hand the influence of using an uneven distribution of the gas through 7 instead of 8 gas inlet slots on the appearance of eigenmodes in the system and segregation (Fig. 15b) and on the other hand the influence of decreasing the number of gas inlet slots to 4 while keeping the total gas flow rate identical on the particle bed uniformity, stability and segregation (Fig. 15c). It can indeed be questioned whether decreasing the number of gas inlet slots from 8 to 4 at given total gas flow rate and as such increasing the gas injection velocity, but decreasing the gas injection uniformity will increase or decrease the ratio of the single particle centrifugal force-to-radial gas-solid drag force and will as such be advantageous or detrimental for segregation. Snapshots after reaching steady state are shown for a case study with $\rho_{p1}/\rho_{p2} = 2$. Fig. 15b shows that reducing the number of gas inlets to 7 by closing one of the gas inlets (top right) allows to eliminate to a large extent and in most of the vortex chamber the previously observed eigenmode and as such to improve the bed uniformity. Only in the top region of the vortex chamber, a distinct non-uniformity in the shape of the inner particle

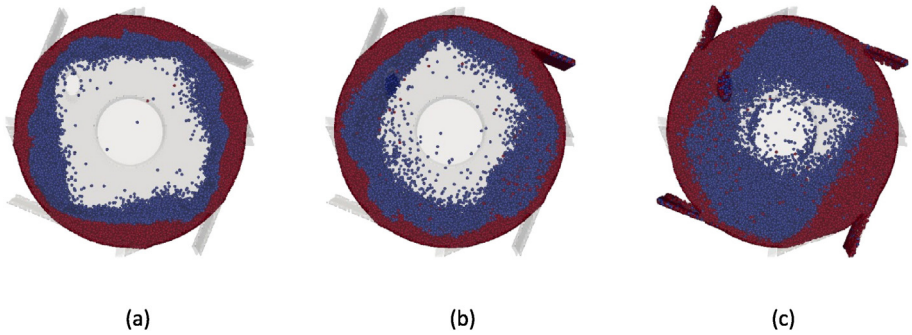

Fig. 15. Influence of the number of gas inlet slots on the steady state profiles of the particle positions and segregation (snapshots shown). Case studies with a particle density ratio (ρ_{p1}/ρ_{p2}) of 2.0 and with (a) 8 slots and $F_g = 8 \times 10$ g/s, (b) 7 slots (1 slot closed) and $F_g = 7 \times 10$ g/s, and (c) 4 slots and $F_g = 4 \times 20$ g/s.

bed is observed, in the particle bed rotation direction downstream of the closed gas inlet. As was shown both numerically and experimentally [12], most of the gas injected via a given gas inlet is rapidly deflected radially inward upon contact with the particle bed and leaves the particle bed before encountering the gas injected via the next gas inlet slot. Gas not coming in via the closed gas inlet slot in Fig. 15b and as such not exerting a radially inward gas-solid drag force on the particles explains the contraction of the particle bed downstream of the closed gas inlet. Fig. 15c demonstrates that further reducing the number of gas inlet slots to 4 is detrimental for the particle bed uniformity and the efficiency of momentum transfer between the injected gas and the particle bed. A new eigenmode is observed and the more pronounced expansion of the inner bed indicates a lower ratio of the single particle centrifugal force-to-radial gas-solid drag force and results in somewhat increased solids losses via the chimney. The observations are in line with the results of simulations by De Wilde et al. [39] using a Eulerian-Eulerian model that showed that an axisymmetric flow pattern cannot be guaranteed in a vortex chamber with 4 gas inlet slots. Despite the more pronounced non-uniformity, segregation is, however, maintained. Comparing the average particle heights and velocities of the heavy and light particles reached at steady state in a vortex chamber with 8 and 4 gas inlet slots, no significant differences are observed (not shown). The variance on the particle heights and velocities increases, however, significantly, as can already be seen from Fig. 15a and c, reflecting the increased large scale non-uniformity. The transient behavior is also quantitatively different with lower frequency fluctuations in the average particle heights and velocities when the number of gas inlet slots is reduced.

5. Conclusions

Simulations of bi-disperse rotating fluidized beds in a vortex chamber are carried out using the MFIX CFD-coarse-grained DPM code. Whereas the density and diameter of the heavy/large particles is kept constant, the density or diameter of the light/small particles is varied. The simulations show that within a couple of cm high vortex chamber generated rotating fluidized bed, three functionalities - high-G intensified gas-solid contact, gas-solids separation and solids-solids segregation - can be effectively combined. Uniform and relatively dense rotating fluidized beds with few losses of particles via the central gas outlet/chimney are obtained in almost all cases. The quality of segregation depends, however, on the particle properties. In general, segregation is seen to be faster and more pronounced with increasing particle density or diameter ratio. With particles of different density, an inner bed of light particles without contamination by heavy particles is easily formed, that is, even with a particle density ratio of 1.35. Evacuation of the light particles from the outer bed of heavy particles requires a somewhat higher density ratio of 2.0. Whereas the density and height of the outer bed are not much affected by the density of the light particles, the height and density of the inner bed are seen to increase, respectively with decreasing density of the light particles. At the higher particle density ratios of 5 and 10, bubble formation in the inner bed is observed along with some losses of light particles via the chimney. The bubbles are seen to intensify the back-mixing of small particles into the outer bed of mainly large particles, so that an optimum particle density ratio for pure segregation exists. Up to a particle density ratio of 2, the difference in the rotation speed of the outer bed of heavy and inner bed of light particles increases with increasing particle density ratio, the outer bed rotating faster and the inner bed slower. When bubbles are formed, the velocity of the inner bed increases and approaches that of the outer bed. High-quality segregation based on size difference only is somewhat more challenging in the centimeters-high bed. Again, an optimum particle diameter ratio for pure segregation exists. With a particle diameter ratio of 2, nearly pure segregation can be achieved. At higher particle diameter ratio, the interface between the outer and inner bed becomes irregular and contamination of both the outer and inner bed with respectively small and large particles increases slightly. Up to a particle diameter ratio of 2.0, the outer and inner average particle height increases respectively decreases with increasing particle diameter ratio, after which they stay nearly constant. Expansion of the inner bed with increasing particle diameter ratio is also observed. At particle diameter ratios above 3, losses of mainly small and some large particles via the chimney are observed. Bubble formation is much less pronounced than in bi-disperse beds with particles of different density. The bed intruding the freeboard region reduces the strength of the central vortex, detrimental for the bed stability. With increasing particle diameter ratio, the average particle velocity of the outer bed increases, whereas that of the inner bed decreases up to a particle diameter ratio of about 2.0, above which the latter again increases. At high particle diameter ratio, the difference between the rotation speed of the outer and inner beds is, however, more pronounced than in a bi-disperse bed of high particle density ratio. A feature of vortex chamber technology is the high flexibility with respect to the gas flow rate, the latter affecting both the centrifugal force and counter-acting radial gas-solid drag force in similar ways. Simulations with doubled gas flow rate show that the influence of the gas flow rate on segregation is indeed minor. Simulations with vortex chambers with 4 and 8 evenly and 7 non-evenly distributed gas inlet slots indicate that the presence of a large-scale non-uniformity in the bed reflects an eigenmode of the system and that a sufficiently high number of gas inlet slots and a sufficiently high gas flow rate are required to achieve uniform operation. Finally, high-G operation opens the way to more precise model validation. The experimental study initiated by Weber et al. [22] will be extended to provide the data of required accuracy.

Vortex chamber generated rotating fluidized beds are not meant to replace conventional fluidized beds for any application. Solids-solids segregation is indeed efficient by the high-G intensified driving force, similar to the functioning of a centrifuge. But the relatively high gas flow rate that is required to keep the bed rotating is an issue. The objective must therefore be to combine efficient segregation with efficient gas-solids contact – and related conversion of the gas and/or solids, as well as with efficient gas-solids separation. In major potential applications (e.g. oxy-fuel combustion), the gas that is fed will, hence, not

only serve driving the bed rotational motion/particle segregation. Efficient gas conversion in relatively thin vortex chamber generated rotating fluidized beds was demonstrated by several groups [10,11,18], despite the typically high gas(-solid slip) velocities and related extremely short gas phase residence times in the bed. This strong performance is due to the high particle bed density and strongly improved particle bed uniformity. The cost in terms of pressure drop also remains relatively small because of the relatively thin bed.

Disclaimer

This report was prepared as an account of work sponsored by an agency of the United States Government. Neither the United States Government nor any agency thereof, nor any of their employees, makes any warranty, express or implied, or assumes any legal liability or responsibility for the accuracy, completeness, or usefulness of any information, apparatus, product, or process disclosed, or represents that its use would not infringe privately owned rights. Reference herein to any specific commercial product, process, or service by trade name, trademark, manufacturer, or otherwise does not necessarily constitute or imply its endorsement, recommendation, or favoring by the United States Government or any agency thereof. The views and opinions of authors expressed herein do not necessarily state or reflect those of the United States Government or any agency thereof.

Acknowledgements

This research was supported in part by an appointment to the National Energy Technology Laboratory Research Participation Program, sponsored by the U.S. Department of Energy and administered by the Oak Ridge Institute for Science and Education. This technical report was produced in support of the National Energy Technology Laboratory's ongoing researchin advanced numerical simulation of multiphase flow underthe RES contract DE-FE0004000. JDW would like to thank Dr. George Richards at NETL for the interesting discussions and continuous follow-up of the research. The authors would like to thank Dr. Sofiane Benyahia at NETL for his collaboration, critical discussion and support.

Appendix A. Supplementary data

Supplementary data to this article can be found online at http://dx.doi.org/10.1016/j.powtec.2017.05.037.

References

[1] L.M. Kochetov, B.S. Sazhin, E.A. Karlik, Experimental determination of the optimal ratios of structural dimensions in the whirl chamber for drying granular materials, Khimicheskoe i Neftyanoe Mashinostroenie 1969, pp. 2–10.
[2] L.M. Kochetov, B.S. Sazhin, E.A. Karlik, Hydrodynamics and heat exchange in vortex drying chambers, Khimicheskoe i Neftyanoe Mashinostroenie 1969, pp. 9–10.
[3] L.A. Anderson, S. Hasinger, B.N. Turman, Two component vortex flow studies, with implications for the colloid core nuclear rocket concept, A.I.A.A. paper, 71, 1971, p. 637.
[4] L.A. Anderson, S. Hasinger, B.N. Turman, Two-component vortex flow studies of the colloid core nuclear rocket, J Spacecr. 9 (5) (1972) 311–317.
[5] W.S. Lewellen, D.B. Stickler, Two-phase vortex investigation related to the colloidal core nuclear reactor, OH, USA: Aerospace Research Laboratory, Wright Patterson Air Force Base;ARL TR, 1972 (72-0037).
[6] D.B. Stickler, H. Lakshmikantha, W.S. Lewellen, Heat transfer and containment processes in two-phase cavity nuclear reactor, Aerospace Research Laboratory, Wright Patterson Air Force Base, OH, USA;ARL TR, 1974 (74-0007).
[7] E.P. Volchkov, V.I. Terekhov, A.N. Kaidanik, A.N. Yadykin, Aerodynamics and heat and mass transfer of fluidized particle beds in vortex chambers, Heat Transfer Eng. 14 (3) (1993) 36–47.
[8] E.P. Volchkov, N.A. Dvornikov, A.N. Yadykin, Characteristic features of heat and mass transfer in a fluidized bed in a vortex chamber, Heat Transfer Res. 34 (7 & 8) (2003) 486–498.
[9] A. de Broqueville, J. De Wilde, Numerical investigation of gas-solid heat transfer in rotating fluidized beds in a static geometry, Chem. Eng. Sci. 64 (6) (2009) 1232–1248.
[10] R.W. Ashcraft, G.J. Heynderickx, G.B. Marin, Modeling fast biomass pyrolysis in a gas-solid vortex reactor, Chem. Eng. J. 207–208 (2012) 195–208.
[11] R.W. Ashcraft, J. Kovacevic, G.J. Heynderickx, G.B. Marin, Assessment of a gas-solid vortex reactor for SO_2/NO_x adsorption from flue gas, Ind. Eng. Chem. Res. 52 (2013) 861–875.
[12] J. De Wilde, Gas-solid fluidized beds in vortex chambers, Chem. Eng. Process. 85 (2014) 256–290.
[13] P. Eliaers, J. De Wilde, Drying of biomass particles: experimental study and comparison of the performance of a conventional fluidized bed and a rotating fluidized bed in a static geometry, Dry. Technol. 31 (2) (2013) 236–245.
[14] P. Eliaers, J.R. Pati, S. Dutta, J. De Wilde, Modeling and simulation of biomass drying in vortex chambers, Chem. Eng. Sci. 123 (2015) 648–664.
[15] P. Eliaers, A. de Broqueville, A. Poortinga, T. van Hengstum, J. De Wilde, High-G, low-temperature coating of cohesive particles in a vortex chamber, Powder Technol. 258 (2014) 242–251.
[16] N. Staudt, A. de Broqueville, W.R. Trujillo, J. De Wilde, Low-temperature pyrolysis and gasification of biomass: numerical evaluation of the process intensification potential of rotating- and circulating rotating fluidized beds in a static fluidization chamber, Int. J. Chem. React. Eng. 9 (2011) (paper A43).
[17] W.R. Trujillo, J. De Wilde, Computational fluid dynamics simulation of fluid catalytic cracking in a rotating fluidized bed in a static geometry, Ind. Eng. Chem. Res. 49 (11) (2010) 5288–5298.
[18] W.R. Trujillo, J. De Wilde, Fluid catalytic cracking in a rotating fluidized bed in a static geometry: a CFD analysis accounting for the distribution of the catalyst coke content, Powder Technol. 221 (2012) 36–46.
[19] A. de Broqueville, Catalytic polymerization process in a vertical rotating fluidized bed. Belgian patent 2004/0186; Internat. Classif.: B01J C08F B01F; Publ. no.: 1015976A3; (2004).
[20] A. de Broqueville, Inventor. Injectors distributed around a fixed wall of a circular reaction chamber inject fluids along this wall in successive layers; one or more fluids entrain solid particles passing through the chamber in rapid rotation to concentrate them along the wall; for catalytic polymerization, drying, impregnating. US patent US2009/0022632; (2009).
[21] J. De Wilde, G. Richards, S. Benyahia, Discrete particle simulations of segregation in a bi-disperse rotating fluidized bed in a vortex chamber, Adv. Powder Technol. 27 (4) (2016) 1453–1463.
[22] J.M. Weber, R.C. Stehle, R.W. Breault, J. De Wilde, Experimental study of the application of rotating fluidized beds to particle separation, Powder Technol. (2017), http://dx.doi.org/10.1016/j.powtec.2016.12.076 (in press).
[23] P.A. Cundall, O.D.L. Strack, A discrete numerical model for granular assemblies, Geotechnique 29 (1979) 47–65, http://dx.doi.org/10.1680/geot. (1979). 29.1.47.
[24] Y. Tsuji, T. Kawaguchi, T. Tanaka, Discrete particle simulation of two-dimensional fluidized bed, Powder Technol. 77 (1993) 79–87, http://dx.doi.org/10.1016/0032-5910(93)85010-7.
[25] R. Garg, J. Galvin, T. Li, S. Pannala, Documentation of Open-source MFIX-DEM Software for Gas-solids Flows, 2010 (https://mfix.netl.doe.gov/documentation/dem_doc_2010).
[26] M. Sakai, M. Abe, Y. Shigeto, S. Mizutani, H. Takahashi, A. Viré, J.R. Percival, J. Xiang, C.C. Pain, Verification and validation of a coarse grain model of the DEM in a bubbling fluidized bed, Chem. Eng. J. 244 (2014) 33–43.
[27] L. Lu, K. Yoo, S. Benyahia, Coarse-grained-particle method for simulation of liquid–solids reacting flows, Ind. Eng. Chem. Res. (2016)http://dx.doi.org/10.1021/acs.iecr.6b02688.
[28] R. Garg, J. Galvin, T. Li, S. Pannala, Open-source MFIX-DEM software for gas–solids flows: part I—verification studies, Powder Technol. 220 (2012) 122–137, http://dx.doi.org/10.1016/j.powtec.2011.09.019.
[29] T. Li, R. Garg, J. Galvin, S. Pannala, Open-source MFIX-DEM software for gas-solids flows: part II — validation studies, Powder Technol. 220 (2012) 138–150, http://dx.doi.org/10.1016/j.powtec.2011.09.020.
[30] B.P.B. Hoomans, J.A.M. Kuipers, W.P.M. van Swaaij, Discrete particle simulation of segregation phenomena in dense gas-fluidized beds, in: L.S. Fan, T.M. Knowlton (Eds.),Fluidization, vol. IX, 1998, pp. 485–492.
[31] G.A. Bokkers, M. van Sint Annaland, J.A.M. Kuipers, Mixing and segregation in a bidisperse gas–solid fluidised bed: a numerical and experimental study, Powder Technol. 140 (3) (2004) 176–186.
[32] Y.Q. Feng, B.H. Xu, S.J. Zhang, A.B. Yu, P. Zulli, Discrete particle simulation of gas fluidization of particle mixtures, AIChE J. 50 (2004) 1713–1728.
[33] O.O. Olaofe, A.V. Patil, N.G. Deen, M.A. van der Hoef, J.A.M. Kuipers, Simulation of particle mixing and segregation in bidisperse gtas fluidized beds, Chem. Eng. Sci. 108 (2014) 258–269.
[34] N. Tagami, A. Mujumdar, M. Horio, DEM simulation of polydisperse systems of particles in a fluidized bed, Particuology 7 (1) (2009) 9–18.
[35] M. Farzaneh, S. Sasic, A. Almstedt, F. Johnsson, D. Pallarès, A novel multigrid technique for Lagrangian modeling of fuel mixing in fluidized beds, Chem. Eng. Sci. 66 (22) (2011) 5628–5637.
[36] H.R. Norouzi, N. Mostoufi, R. Sotudeh-Gharebagh, Effect of fines on segregation of binary mixtures in gas–solid fluidized beds, Powder Technol. 225 (2012) 7–20.
[37] J.F. Dietiker, C. Guenther, M. Syamlal, A Cartesian cut cell method for gas/solids flows, AIChE Annual Meeting. Nashville, TN, 2009.
[38] M.J.V. Goldschmidt, J.M. Link, S. Mellema, J.A.M. Kuipers, Digital image analysis measurements of bed expansion and segregation dynamics in dense gas-fluidised beds, Powder Technol. 138 (2–3, 10) (2003) 135–159.
[39] J. De Wilde, A. Habibi, A. de Broqueville, Experimental and numerical study of rotating fluidized beds in a static geometry, Int. J. Chem. React. Eng. 5 (2007), A106.